

# Recent Progress in High Resolution 2D Imaging Measurements of Reconnection Heating during Merging Plasma Startup in TS-3<sup>\*)</sup>

Hiroshi TANABE, Qinghong CAO<sup>1)</sup>, Haruaki TANAKA, Tara AHMADI<sup>1)</sup>, Moe AKIMITSU, Asuka SAWADA, Michiaki INOMOTO and Yasushi ONO

*Graduate School of Frontier Sciences, University of Tokyo, Tokyo 113-0032, Japan*

<sup>1)</sup>*Graduate School of Engineering, University of Tokyo, Tokyo 113-0032, Japan*

(Received 11 January 2019 / Accepted 21 April 2019)

We present recent results from high resolution 2D imaging measurement of reconnection heating during central solenoid (CS)-free merging startup of spherical tokamak plasmas in TS-3 using an ultra-high resolution 2D ion Doppler tomography and in-situ 2D magnetic probe arrays. The new high-resolution 2D ion Doppler tomography diagnostic has successfully resolved the formation of fine structure during magnetic reconnection and it has been found that magnetic reconnection increases the ion temperature inside a current sheet as well as in the downstream region of an outflow jet. The maximum ion temperature is obtained during a current sheet ejection event and the double peak structure of ion heating becomes clearer after the end of reconnection. The maximum ion heating increases with the reconnecting magnetic field. The high temperature region in the downstream typically propagates vertically along a closed flux surface and MAST-like fine structure formation has successfully been reproduced in this laboratory experiment for the first time.

© 2019 The Japan Society of Plasma Science and Nuclear Fusion Research

Keywords: spherical tokamak, CS-free startup, magnetic reconnection, ion heating, guide field

DOI: 10.1585/pfr.14.3401110

## 1. Introduction

Magnetic reconnection is a fundamental process which accelerates and heats plasmas through the rearrangement of magnetic field lines. It is known to be an effective way of converting magnetic energy into plasma thermal energy in proportion to the square of the reconnecting magnetic field. Magnetic reconnection is observed in many fusion, laboratory and astrophysical plasmas such as geomagnetic substorms in the Earth's magnetosphere, solar flares and sawtooth crashes in tokamaks [1, 2]. In the 1990's, application of the self-organizing process was pioneered in TS-3 and START, with significant ion heating of up to  $\sim 200$  eV and several high beta records for spherical tokamak [3–5].

In the last three decades, magnetic reconnection was investigated in a number of experiments: MRX [6–8], SSX [9, 10], VTF [11], TS-4 [12], UTST [13, 14], C-2U [15, 16] and MAST [17–21]. For all of them, the following common characteristics have been reported: (i) magnetic reconnection heats ions downstream and electrons around the X-point where magnetic field lines reconnect [18, 22], (ii) ions are heated by the thermalization of flow energy associated with reconnection outflow [23, 24] while electrons gain energy mostly by Ohmic dissipation of a current sheet [22], (iii) most of the heating energy goes to ions and

electron heating is small [25, 26] (ions are heated globally but electron heating is localized around X-point); and (iv) the maximum heating rate depends on the amplitude of the reconnecting component of magnetic field:  $B_{rec}$  ( $B_p$  for tokamaks) [27]. Significant plasma heating to temperature exceeding 100 eV was demonstrated in many merging experiments such as TS-3 [3], START [28], C-2U [16] and MAST [29].

The high field merging/reconnection experiment in MAST resulted in ion temperatures of  $\sim 1$  keV and bulk electron heating to temperatures upto hundreds of eV through ion-electron energy relaxation [29–31], successfully exceeding radiation losses due to low-Z impurities to achieve plasma duration times of over 100 ms in the central solenoid (CS)-free startup [27, 31]. As a promising startup scenario for spherical tokamak, the high field merging experiment in MAST was also successfully combined with additional heating by NBI and a solenoid (hybrid startup scenario) to establish H-mode and higher/longer flat-top plasma current (typically hundreds of milliseconds) [27, 31, 32]. In the MAST merging experiments, which typically operated in high guide field conditions  $B_t/B_{rec} > 3$  with  $B_t \sim 0.6$  T and  $B_{rec} \sim 0.1$  T [33], better ion energy confinement after merging helps to combine high temperature merging plasma startup with long pulse scenarios.

However in MAST, due to the absence of in-situ magnetic field measurements during reconnection, investiga-

author's e-mail: [tanabe@ts.t.u-tokyo.ac.jp](mailto:tanabe@ts.t.u-tokyo.ac.jp)

<sup>\*)</sup> This article is based on the invited presentation at the 27th International Toki Conference (ITC27) & the 13th Asia Pacific Plasma Theory Conference (APPTC2018).

tion of the detailed heating/transport mechanism was not possible. The clear results from 130CH-YAG/300CH-Ruby Thomson scattering [34–37] and 32CH ion Doppler tomography diagnostics [38,39] provided new insights into magnetic reconnection, fine structure formation such as highly peaked structure around  $X$ -point and poloidally-ring-like hollow ion temperature profile [33] by the coupling of outflow heating mechanism and toroidal confinement [18], but those processes have not yet been investigated comprehensively due to the absence of proper magnetic diagnostics. Based on the feedback, a recent TS-3 experiment made a further diagnostics upgrade for MAST-like high resolution imaging measurement and has started detailed investigation of guide field reconnection with a guide field ratio similar to that in MAST. This summary paper on an invited talk at ITC-27 provides a brief summary of the high guide field reconnection experiment in TS-3 (section 2). We then focus on impulsive heating events associated with current sheet ejection in section 3. Detailed measurements of the time-evolving ion temperature profile around the  $X$ -point reveals fine structure both inside diffusion region and downstream of magnetic reconnection. The characteristic hot spots formed by reconnection heating are successfully trapped by the thick layer of closed flux surface and then equilibrated/transported to form poloidally-ring-like hollow distribution after the end of merging.

## 2. Merging Plasma Startup of Spherical Tokamak in TS-3

Figure 1 shows the schematic view of merging plasma startup device TS-3 [40,41]. TS-3 has a CS/TF coil at the

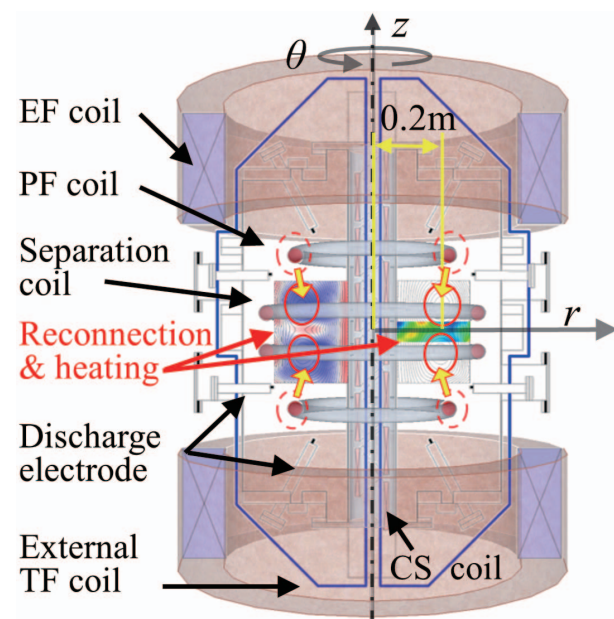


Fig. 1 Plasma merging device TS-3. Two internal PF coils drive magnetic reconnection.

center of the machine ( $R_{CS} = 0.06$  m: typically  $I_{TF} \sim 50$  kA · turn and  $I_{CS} = 0$  kA (CS-free scenario)), a pair of EF (equilibrium field coils:  $R_{EF} \sim 0.5$  m and 234 turns: typically  $I_{EF} \sim 0.1$  kA in DC), PF ( $R_{PF} \sim 0.22$  m and 4 turns), separation coils ( $R_{sep} \sim 0.31$  m and 3 turns) and discharge electrodes (used for preliminary discharge). The cylindrical vacuum vessel has  $R_{wall} = 0.375$  m and 1.17 m long. It is a relatively small scale laboratory experiment like START [4,28,42].

Figure 2 illustrates a typical operation scenario of CS-free merging plasma startup [14,22] in TS-3. As shown in fast camera images (*Photron: SA-Z*), initial two plasma rings (hydrogen) are generated at the top and bottom of the device by the induction of two internal PF coils. When the polarity of  $I_{PF}$  is reversed, the negative current contributes to detachment of the plasma rings from PF coils and pushes the two plasma tori vertically toward midplane. In addition to the rapid increment of plasma current, magnetic reconnection occurs with characteristic bright structure [43–45] around the  $X$ -point at  $t \sim 75$   $\mu$ s. Merging finishes roughly around  $t \sim 80$   $\mu$ s and finally a spherical tokamak configuration is formed with additional shaping by separation coil current  $I_{sep}$ . The evolution of poloidal flux profile was measured by 2D (60CH) internal magnetic probe arrays [3,22] whose minimum interval is  $dz \sim 10$  mm and

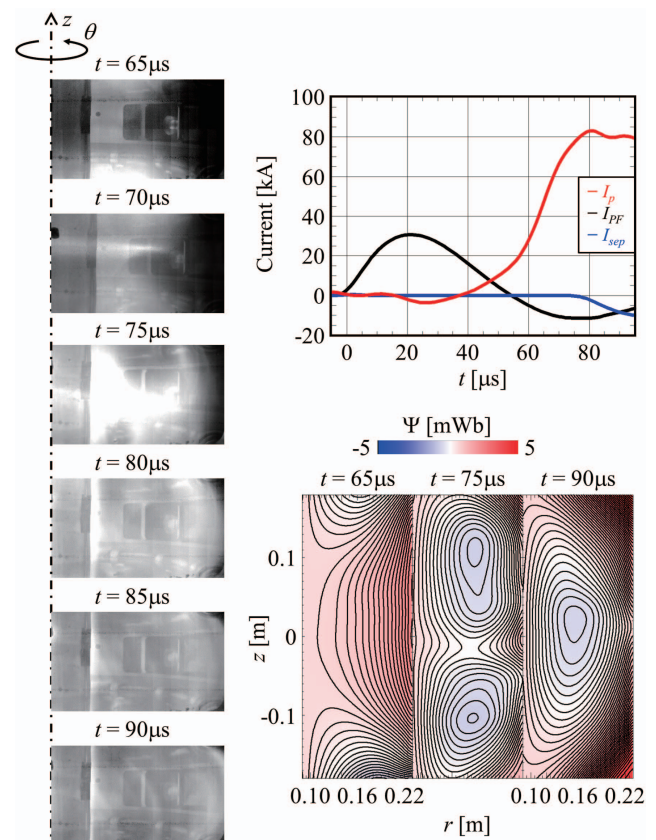


Fig. 2 Typical feature of merging plasma startup of spherical tokamak in TS-3: high speed video images, operational waveforms and poloidal flux profile.

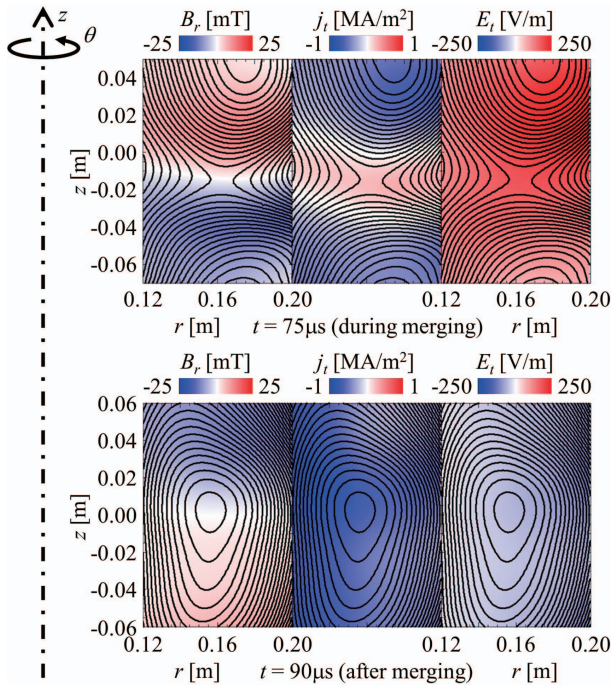


Fig. 3 Typical profile of radial component of magnetic field, current density and toroidal electric field around X-point.

$dr \sim 40$  mm around X-point. Ion heating was monitored by following two types of new upgraded ion Doppler tomography diagnostics: a 1D (15CH) high-speed system ( $dr \sim 10$  mm,  $10 \mu\text{s}/\text{frame}$  and  $d\lambda \sim 0.0054$  nm/pixel by a  $f = 0.5$  m spectrometer ( $g = 1800$  L/mm) and an image-intensified CMOS fast camera) and a 2D (96CH) imaging system ( $dr \sim 10$  mm and  $d\lambda \sim 0.0048$  nm/pixel with a  $f = 1.0$  m spectrometer ( $g = 2400$  L/mm) and an ICCD camera).

Figure 3 shows typical magnetic field configuration during tokamak merging in TS-3 [25]. The color contours illustrates radial component of magnetic field  $B_{rec}$ , toroidal current density  $j_t$  and toroidal electric field  $E_t$ . During merging/reconnection, it typically has double magnetic axes at the top and bottom of the device and a X-point around the midplane. The radial component of poloidal magnetic field  $B_r$  is one of the most important components of the reconnecting magnetic field  $B_{rec}$  which determines the amplitude of reconnection heating and final temperature obtained by merging plasma startup [22, 27]. Toroidal current density  $j_t$  typically has opposite polarity around X-point, forming a current sheet [22, 25], and the structure disappears after merging. The toroidal electric field is calculated from the time-derivative of poloidal flux and we refer to it as the reconnecting electric field  $E_{rec}$  because it characterizes the speed of the topology change during reconnection. As shown in Fig. 3, the plasma shots used in this paper are in the regime of relatively small reconnecting magnetic field  $B_{rec} = B_r \sim 0.02$  T and higher guide field ratio with limited toroidal magnetic field  $B_t \sim 0.1$  T ( $B_t/B_{rec} \sim 5$ ).

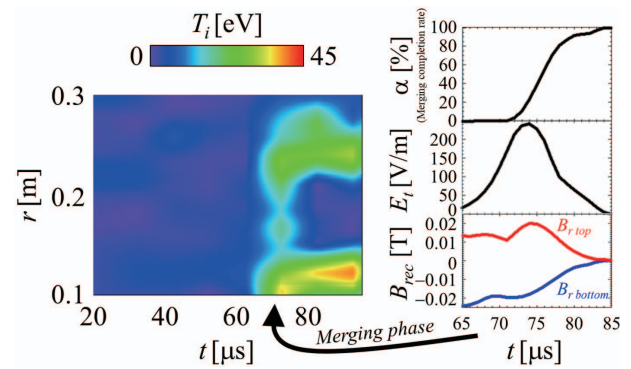


Fig. 4 Time evolution of ion heating during magnetic reconnection in TS-3 and reference time evolution of merging completion ratio  $\alpha$  [%], toroidal electric field  $E_t$  (reference of reconnection speed) and reconnecting magnetic field component  $B_{rec} = B_r$ .

### 3. Ion Heating and Transport Process during Tokamak Merging in TS-3

Figure 4 (left) shows time evolution of ion temperature profile during merging plasma startup in TS-3 and Fig. 4 (right) illustrates the reference time scale of merging completion ratio  $\alpha$  [%], toroidal electric field  $E_t = -(\partial\psi/\partial t)/2\pi r$  (rate of flux changes: reconnection speed) and the amplitude of reconnecting (poloidal) magnetic field component  $B_{rec} = B_r \sim 0.02$  T. Ion temperature increases around  $t = 70 \sim 80 \mu\text{s}$  when  $\alpha$  rapidly changes with corresponding higher reconnecting electric field  $E_t$ . Ion temperature mainly increases in the downstream region of reconnection by outflow heating mechanism and the amplitude of the heating is in the order of flow energy of poloidal Alfvén speed ( $V_{p,Alfvén} \sim 50$  km/s with  $B_{rec} \sim 0.02$  T) [25].

Figure 5 shows the detailed time evolution of 2D toroidal current density and ion temperature profile around X-point during the rapid temperature rise from  $t = 72 \mu\text{s}$  to  $t = 82 \mu\text{s}$ . During magnetic reconnection, initially anti-parallel toroidal current is formed around the X-point. The anti-parallel current structure which has opposite polarity with plasma current starts to dissipate after  $t = 74 \mu\text{s}$  and forms double peak structure at  $t = 76 \mu\text{s}$ . Those two peaks are ejected radially (“current sheet ejection” [46, 47]) at  $t = 78 \mu\text{s}$  and the merging process completes after that. The ion heating structure shows similar characteristics during reconnection. Before merging, the ion temperature is just a few eV but it starts to increase at  $t = 74 \mu\text{s}$  initially around the current sheet. The high temperature region spreads horizontally toward outflow direction at  $t = 76 \mu\text{s}$  and the downstream high  $T_i$  region propagates vertically downstream aligned with field line direction. At  $t = 78 \mu\text{s}$ , the ion temperature reaches its maximum value of over 25 eV when the current sheet is completely ejected from the X-point. After that, the two magnetic axes of merging tori approach the midplane and push the double peak structure radially. The outboard ejection stagnates

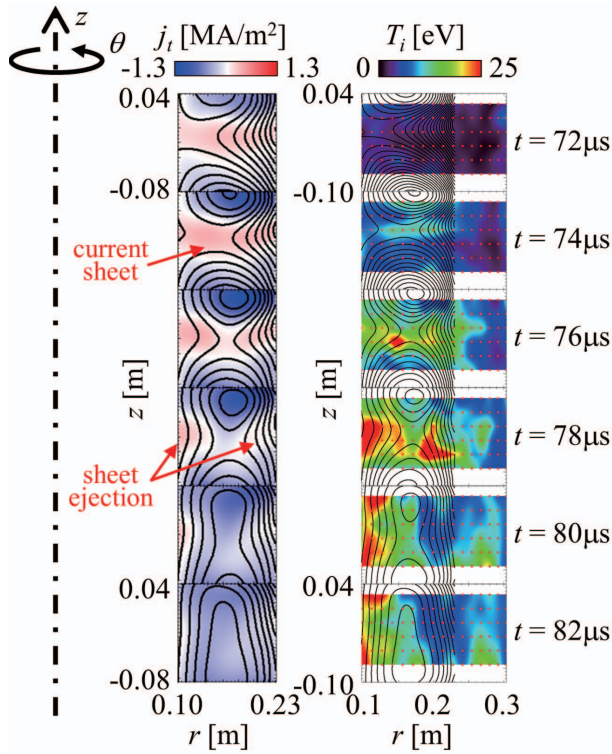


Fig. 5 Detailed 2D imaging measurement of current density/flux and ion temperature profile during the double peak structure formation process by outflow heating and current sheet ejection.

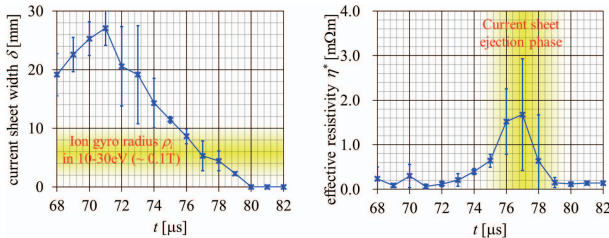


Fig. 6 Time evolution of the half width of current sheet thickness  $\delta$  at the X-point and effective resistivity  $\eta^*$  during merging. When the current sheet separates to form a double peak structure, its half width at the X-point becomes comparable to the ion Larmor radius  $\rho_i$ , and a significant increase of effective resistivity is observed at this phase.

around  $r \sim 0.28$  m and a clear double peak structure is obtained after merging.

Figure 6 illustrates the time evolution of current sheet thickness  $\delta$  evaluated at the X-point and effective resistivity  $\eta^* = E_t/j_t$ . During guide field reconnection, the ion gyro radius  $\rho_i$  tends to be smaller than the current sheet thickness and meandering motion is initially suppressed. However, when current sheet ejection is triggered, the thickness of the diffusion region around the X-point becomes comparable to the ion gyro radius. The apparent reconnection speed  $E_{rec}$  is not maximum at this time but the effective resistivity increases to a much higher value than the

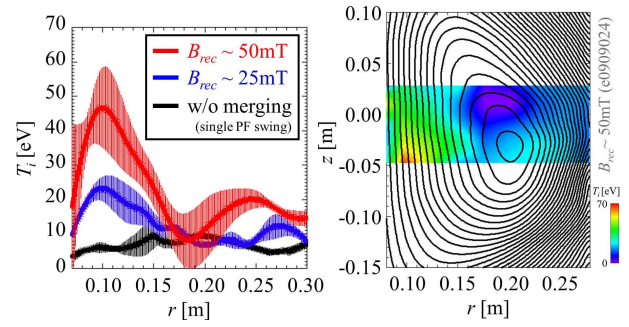


Fig. 7 Comparison of reconnection heating when merging ratio reaches  $\alpha \sim 100\%$  and reference global geometry with 2D ion temperature profile. At the end of reconnection, the double peak structure is surrounded by thick layer of closed flux surface.

classical resistivity  $\eta_{Spitzer} \sim 10^{-2}$  [m $\Omega\text{m}$ ]. Although the radial spatial resolution of the magnetic probes is not sufficient to detect the radial motion of the split current sheet, *Akimitsu* [48] reported associated island structure formation and ejection-like features, detected by developing new PCB-type radially high-resolution magnetic sensors. Ion temperature rapidly increases during the ejection event and its profile changes to a double peak structure at the end of merging.

Figure 7 shows the dependence of ion heating on reconnecting field  $B_{rec}$ . At the end of merging ( $\alpha \sim 100\%$ ), reconnection outflow and current sheet ejection initially forms a double peak structure of ion temperature profile downstream. In comparison with counter-helicity merging of spheromaks [41], which involves the collision of two spheromaks with opposite toroidal magnetic field polarity and resulted in maximum ion temperature up to  $\sim 250$  eV in the 1990's [3], the obtained maximum reconnection heating is smaller for tokamak merging. One of the major difference is the available magnetic energy which is released during magnetic reconnection. In co-helicity type reconnection [49, 50] (spheromak-spheromak or tokamak-tokamak merging with same polarity of toroidal magnetic field), the reconnecting magnetic field component is the poloidal magnetic field and the toroidal field does not dissipate during reconnection. In counter helicity merging, on the other hand, the toroidal field also contributes to the reconnection process and it drives outflow acceleration in the toroidal direction, so called the sling-shot effect [3, 49]. The sheared toroidal rotation dissipates around the magnetic axis after merging, and the final temperature tends to form a parabolic profile with the maximum value around the null-point; in contrast, co-helicity merging typically forms a hollow distribution as shown in Fig. 7 and [50–52]. Although the amplitude of ion heating is smaller for co-helicity reconnection, tokamak merging has the advantage of better plasma confinement via the toroidal magnetic field. Without a guide field, the ratio of parallel/perpendicular ion heat diffusivity typically has a small

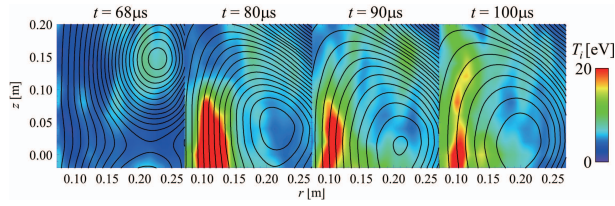


Fig. 8 Global 2D ion temperature profile measurement before and after merging in TS-3U. Upstream plasma initially has singly peaked distribution but magnetic reconnection changes the profile to form a high temperature region downstream. The new experiment successfully demonstrated/visualized that the impulsively formed high temperature region downstream is successfully confined inside the closed flux surface and equilibrated to form poloidally-ring-like hollow distribution mostly by parallel heat transport process.

value ( $\chi_{\parallel}^i/\chi_{\perp}^i \sim 1$  in MRX [53]) and the strong heat flux driven by  $-\nabla T_i$  propagates directly in the radial direction. However, under the influence of higher toroidal guide field in tokamak merging,  $\chi_{\parallel}^i/\chi_{\perp}^i \sim 2(\omega_{ci}\tau_{ii})^2 > 10$  is typically satisfied and most of the heat flux driven by ion temperature gradient propagates vertically on the thick layer of closed flux surface because perpendicular heat conduction is strongly suppressed in the presence of higher toroidal magnetic field. In addition, the amplitude of downstream heating could be increased by having a higher poloidal magnetic field in the upstream plasma. Tokamak merging leads to high confinement as a trade off against strong heating.

Nevertheless, previous TS-3 experiments have not investigated detailed heat transport processes after merging because the possible diagnostics access for ion temperature measurement was limited to  $-75 \text{ mm} < z < 25 \text{ mm}$  due to the finite size of the midplane window. In 2018, the access was improved by upgrading the vacuum vessel to TS-3U (TS-6). It reuses the same PF coils as TS-3 ( $\tau_{PF} \sim 100 \mu\text{s}$  as in Fig. 2) for the initial campaign and its merging time scale is nearly the same as that of TS-3. Figure 8 shows the global time evolution of the 2D ion temperature profile before and after merging measured in the new device with 2D (150CH) internal magnetic probe arrays. In TS-3, it was assumed that reconnection heating profile is quickly equilibrated in a few microseconds on the closed flux surface because the thermal speed of hydrogen plasma is high:  $v_{i,th} \sim 50 \text{ km/s} = 50 \text{ mm}/\mu\text{s}$ . However the actual thermal transport process is not 2D and it is affected by the toroidal configuration (actual propagation path of parallel heat transport is rotated toroidally), finite delay of equilibration was resolved with the detailed measurement in TS-3U. The poloidally localized high temperature region propagates vertically with finite delay time and forms poloidally-ring-like distribution via heat transport processes [51,52]. Under the influence of higher guide fields ( $B_t/B_{rec} \sim 5$  and  $B_t \sim 0.1 \text{ T}$  around the X-point ( $r \sim$

$0.2 \text{ m}$ )), parallel heat transport dominates the equilibration process and perpendicular heat conduction is strongly suppressed by the toroidal magnetic field. The ratio of parallel/perpendicular heat diffusivity  $\chi_{\parallel}^i/\chi_{\perp}^i \sim 2(\omega_{ci}\tau_{ii})^2$  strongly depends on the guide field and it exceeds 100 on the high field side ( $B_t \sim 0.2 \text{ T}$  at  $r \sim 0.1 \text{ m}$ ). In comparison with a no guide field experiment ( $\chi_{\parallel}^i/\chi_{\perp}^i \sim 1$  [53]), tokamak merging typically satisfies  $\chi_{\parallel}^i/\chi_{\perp}^i > 10$  even on the low field side and has a characteristic hollow distribution. Although the initial heating profile is poloidally localized and is not necessary symmetric (typically high temperatures occur in high field side because of a smaller volume in the toroidal configuration and radially asymmetric acceleration [54–56]), its equilibration process to form poloidally-ring-like hollow distribution has successfully been visualized/demonstrated as shown in Fig. 8.

## 4. Summary and Conclusion

Recent clear 2D imaging measurements of ion heating during merging/reconnection plasma startup of spherical tokamak has been briefly reviewed in the paper. Recent new findings and achievement from TS-3 experiment are summarized as follows:

- Merging plasma startup successfully demonstrates CS-free plasma startup for spherical tokamak by utilizing reconnection heating
- Guide field reconnection forms fine structures both around the X-point and in the downstream region
- In tokamak merging, the radial component of the poloidal magnetic field contributes to the heating as a reconnecting magnetic field
- Ions are heated during a fast reconnection phase and the ion temperature typically forms a double peak structure after current sheet ejection
- During current sheet ejection, the thickness of the current sheet at the X-point becomes comparable to the ion gyro radius and a significant increase of the effective resistivity occurs
- After merging, the double peak high temperature region propagates vertically on the closed flux surface of the spherical tokamak and finally forms a poloidally-ring-like characteristic hollow distribution

The recent advances of MAST-like high-resolution plasma diagnostics in laboratory experiments successfully lead to the new finding of fine structure formation during merging plasma startup of spherical tokamak. In addition to the magnetic characteristics of current sheet ejection, a clear double peak ion heating structure formation has successfully been detected synchronized with the magnetic features. The measured ion temperature profile successfully reproduces the fine structure obtained in MAST and it has been established that the poloidally-ring-like temperature structure is aligned with closed flux surfaces by direct measurement of the magnetic field. Although the equilibra-

tion process itself is not necessary surprising, it should be noted as an important milestone that the new experiment has clearly demonstrated/visualized the successful confinement of high power reconnection heating on the closed flux surface of merging startup spherical tokamak.

## Acknowledgement

This work was supported by Grant-in-Aid for Scientific Research 15H05750, 17H04863, 18K18747 and 19H01866, and NIFS Collaboration Research Programs (NIFS16KLER048, NIFS17KNSS091 and NIFS17KKGR006).

- [1] M. Yamada, R. Kulsrud and H. Ji, *Rev. Mod. Phys.* **82**, 603 (2010).
- [2] E.G. Zweibel and M. Yamada, *Annu. Rev. Astron. Astrophys.* **47**, 291 (2009).
- [3] Y. Ono, M. Yamada, T. Akao, T. Tajima and R. Matsumoto, *Phys. Rev. Lett.* **76**, 3328 (1996).
- [4] M. Gryaznevich, R. Akers, P.G. Carolan, N.J. Conway, D. Gates, A.R. Field, T.C. Hender, I. Jenkins, R. Martin, M.P.S. Nightingale, C. Ribeiro, D.C. Robinson, A. Sykes, M. Tournianski, M. Valovic and M.J. Walsh, *Phys. Rev. Lett.* **80**, 3972 (1998).
- [5] Y. Ono, T. Kimura, E. Kawamori, Y. Murata, S. Miyazaki, Y. Ueda, M. Inomoto, A.L. Balandin and M. Katsurai, *Nucl. Fusion* **43**, 789 (2003).
- [6] M. Yamada, H. Ji, S. Hsu, T. Carter, R. Kulsrud, N. Bretz, F. Jobes, Y. Ono and F. Perkins, *Phys. Plasmas* **4**, 1936 (1997).
- [7] J. Yoo, M. Yamada, H. Ji, J. Jara-Almonte, C.E. Myers and L.J. Chen, *Phys. Rev. Lett.* **113**, 095002 (2014).
- [8] J. Yoo, M. Yamada, H. Ji, J. Jara-Almonte and C.E. Meyers, *Phys. Plasmas* **21**, 055706 (2014).
- [9] M.R. Brown, *Phys. Plasmas* **6**, 1717 (1999).
- [10] T. Gray, V.S. Lukin, M.R. Brown and C.D. Cothran, *Phys. Plasmas* **17**, 102106 (2010).
- [11] J. Egedal, A. Fasoli, M. Porkolab and D. Tarkowski, *Rev. Sci. Instrum.* **71**, 3351 (2000).
- [12] H. Tanabe, H. Oka, M. Annoura, A. Kuwahata, K. Kadowaki, Y. Kaminou, S. You, A. Balandin, M. Inomoto and Y. Ono, *Plasma Fusion Res.* **8**, 2405088 (2013).
- [13] T. Yamada, R. Imazawa, S. Kamio, R. Hihara, K. Abe, M. Sakumura, Q. CAO, T. Oosako, H. Kobayashi, T. Wakatsuki, B. AN, Y. Nagashima, H. Sakakita, H. Koguchi, S. Kiyama, Y. Hirano, M. Inomoto, A. Ejiri, Y. Takase and Y. Ono, *Plasma Fusion Res.* **5**, S2100 (2010).
- [14] M. Inomoto, T.G. Watanabe, K. Gi, K. Yamasaki, S. Kamio, R. Imazawa, T. Yamada, X. Guo, T. Ushiki, H. Ishikawa, H. Nakamata, N. Kawakami, T. Sugawara, K. Matsuyama, K. Noma, A. Kuwahata and H. Tanabe, *Nucl. Fusion* **55**, 033013 (2015).
- [15] M.W. Binderbauer *et al.*, *AIP Conf. Proc.* **1721**, 030003 (2016).
- [16] H. Gota *et al.*, *Nucl. Fusion* **57**, 116021 (2017).
- [17] A. Kirk *et al.*, *Nucl. Fusion* **57**, 102007 (2017).
- [18] H. Tanabe *et al.*, *Phys. Rev. Lett.* **115**, 215004 (2015).
- [19] M. Gryaznevich, V. Shevchenko and A. Sykes, *Nucl. Fusion* **46**, S573 (2006).
- [20] M. Gryaznevich, R.J. Akers, G.F. Counsell, G. Cunningham, A. Dnestrovskij, A.R. Field, T.C. Hender, A. Kirk, B. Lloyd, H. Meyer, A.W. Morris, A. Sykes, A. Tabasso, M. Valovic, G.M. Voss, H.R. Wilson and the MAST and NBI teams, *Phys. Plasmas* **10**, 1803 (2003).
- [21] K.G. McClements and M.R. Turnyanskiy, *Plasma Phys. Control. Fusion* **59**, 014012 (2017).
- [22] Y. Ono, H. Tanabe, Y. Hayashi, T. Ii, Y. Narushima, T. Yamada, M. Inomoto and C.Z. Cheng, *Phys. Rev. Lett.* **107**, 185001 (2011).
- [23] J. Yoo, M. Yamada, H. Ji and C.E. Myers, *Phys. Rev. Lett.* **110**, 215007 (2013).
- [24] S.C. Hsu, G. Fiksel, T.A. Carter, H. Ji, R.M. Kulsrud and M. Yamada, *Phys. Rev. Lett.* **84**, 3859 (2000).
- [25] Y. Ono, H. Tanabe, T. Yamada, K. Gi, T. Watanabe, T. Ii, M. Gryaznevich, R. Scannell, N. Conway, B. Crowley and C. Michael, *Phys. Plasmas* **22**, 055708 (2015).
- [26] M. Yamada, J. Yoo, J. Jara-Almonte, H. Ji, R.M. Kulsrud and C.E. Myers, *Nat. Commun.* **5**, 4774 (2014).
- [27] H. Tanabe *et al.*, *Nucl. Fusion* **57**, 056037 (2017).
- [28] M. Gryaznevich and A. Sykes, *Nucl. Fusion* **57**, 072003 (2017).
- [29] Y. Ono, H. Tanabe, T. Yamada, M. Inomoto, T. Ii, S. Inoue, K. Gi, T. Watanabe, M. Gryaznevich, R. Scannell, C. Michael and C.Z. Cheng, *Plasma Phys. Control. Fusion* **54**, 124039 (2012).
- [30] T. Yamada, H. Tanabe, T.G. Watanabe, Y. Hayashi, R. Imazawa, M. Inomoto, Y. Ono, M. Gryaznevich, R. Scannell, C. Michael and the MAST team, *Nucl. Fusion* **56**, 106019 (2016).
- [31] M. Gryaznevich, *IEEE Trans. Fund. Mater.* **125**, 881 (2005).
- [32] A. Sykes *et al.*, *Nucl. Fusion* **41**, 10 (2001).
- [33] H. Tanabe *et al.*, *Phys. Plasmas* **24**, 056108 (2017).
- [34] R. Scannell, M.J. Walsh, M.R. Dunstan, J. Figueiredo, G. Naylor, T. O’Gorman, S. Shibaev, K.J. Gibson and H. Wilson, *Rev. Sci. Instrum.* **81**, 10D520 (2010).
- [35] M.J. Walsh, E.R. Arends, P.G. Carolan, M.R. Dunstan, M.J. Forrest, S.K. Nielsen and R. O’Gorman, *Rev. Sci. Instrum.* **74**, 1663 (2003).
- [36] T. O’Gorman, P.J. Mc Carthy, S. Prunty, M.J. Walsh, M.R. Dunstan, R.B. Huxford, G. Naylor, E. Maguet, R. Scannell and S. Shibaev, *Rev. Sci. Instrum.* **81**, 123508 (2010).
- [37] E.R. Arends, Ph.D. thesis, Eindhoven University of Technology, 2003 (<https://www.differ.nl/node/1512>).
- [38] H. Tanabe, T. Yamada, T. Watanabe, K. Gi, K. Kadowaki, M. Inomoto, R. Imazawa, M. Gryaznevich, R. Scannell, N. Conway, B. Crowley, K.G. McClements, I. Fitzgerald, C. Michael, J. Harrison, A. Meakins, N. Hawkes, T. O’Gorman, C.Z. Cheng and Y. Ono, *Plasma Fusion Res.* **11**, 1302093 (2016).
- [39] H. Tanabe, A. Kuwahata, H. Oka, M. Annoura, H. Koike, K. Nishida, S. You, Y. Narushima, A. Balandin, M. Inomoto and Y. Ono, *Nucl. Fusion* **53**, 093027 (2013).
- [40] Y. Ono, A. Yumoto and M. Katsurai, in *Proceedings of the 1986 IEEE International Conference on Plasma Science, Saskatoon, Canada, 1986* (IEEE, New York, 1986), p.77.
- [41] Y. Ono, A. Morita, M. Katsurai and M. Yamada, *Phys. Fluids B* **5**, 3691 (1993).
- [42] A. Sykes *et al.*, *Nucl. Fusion* **32**, 694 (1992).
- [43] K. Yamasaki, S. Inoue, S. Kamio, T.G. Watanabe, T. Ushiki, X. Guo, T. Sugawara, K. Matsuyama, N. Kawakami, T. Yamada, M. Inomoto and Y. Ono, *Phys. Plasmas* **22**, 101202 (2016).
- [44] T. Ushiki, M. Inomoto, K. Yamasaki, X. Guo, T. Sugawara, K. Matsuyama, H. Koguchi and T. Yamada, *Plasma Fusion Res.* **11**, 2402100 (2016).

- [45] X. Guo, M. Inomoto, T. Sugawara, K. Yamasaki, T. Ushiki, Y. Ono and TS Group, *Phys. Plasmas* **22**, 101201 (2016).
- [46] Y. Ono, Y. Hayashi, T. Ii, H. Tanabe, S. Ito, A. Kuwahata, T. Ito, Y. Kamino, T. Yamada, M. Inomoto and TS-Group, *Phys. Plasmas* **18**, 111213 (2011).
- [47] M. Inomoto, S. Kamio, A. Kuwahata, T.G. Watanabe, K. Yamasaki *et al.*, *Plasma Fusion Res.* **8**, 240112 (2013).
- [48] M. Akimitsu, Y. Ono, Q. Cao and H. Tanabe, *Plasma Fusion Res.* **13**, 1202108 (2018).
- [49] Y. Ono, M. Inomoto, T. Okazaki and Y. Ueda, *Phys. Plasmas* **4**, 1953, (1997).
- [50] R. Horiuchi, T. Morita and S. Usami, *Plasma Fusion Res.* **13**, 3403035 (2018).
- [51] A. Stanier, Ph.D. thesis, The University of Manchester, 2013, p.203. (<https://www.escholar.manchester.ac.uk/jrnl/item/?pid=uk-ac-man-scw:211308>).
- [52] P.K. Browning, S. Cardnell, M. Evans, F. Arese Lucini, V.S. Lukin, K.G. McClements and A. Stanier, *Plasma Phys. Control. Fusion* **58**, 014041 (2016).
- [53] A. Kuritsyn, Ph.D. thesis, Princeton University, 2005, p.125.
- [54] K. Kadowaki, M. Inomoto and Y. Ono, *IEEJ Trans. Fund. Mater.* **132**, 9 (2012).
- [55] S. Kamio, M. Inomoto, K. Yamasaki, T. Yamada, C.Z. Cheng and Y. Ono, *Phys. Plasmas* **25**, 012126 (2018).
- [56] M. Inomoto, A. Kuwahata, H. Tanabe, Y. Ono and TS Group, *Phys. Plasmas* **20**, 061209 (2013).